In Situ *Micro-mechanical Testing of a PM Nickel-Base Superalloy Weld*

K. M. Oluwasegun, J. O. Olawale, G. M. Oyatogun, M. D. Shittu, O. O. Ige & B. O. Malomo

Metallurgical and Materials Transactions A

ISSN 1073-5623
Volume 45
Number 11

Metall and Mat Trans A (2014)
45:5127-5137
DOI 10.1007/s11661-014-2462-3

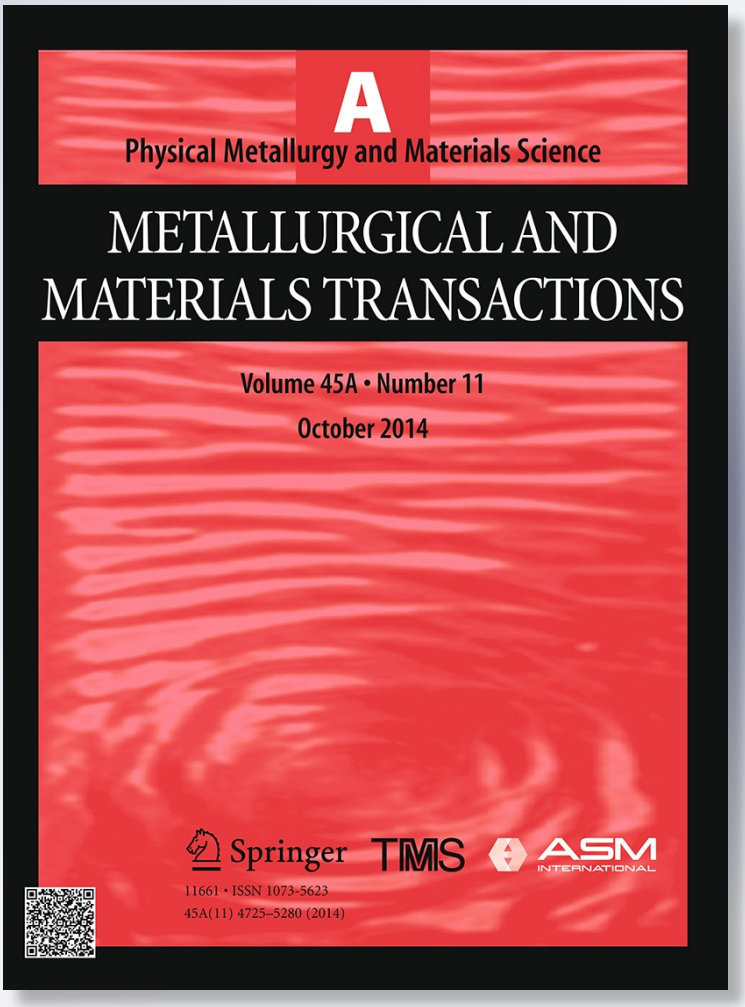

Springer

In Situ Micro-mechanical Testing of a PM Nickel-Base Superalloy Weld

K.M. OLUWASEGUN, J.O. OLAWALE, G.M. OYATOGUN, M.D. SHITTU, O.O. IGE, and B.O. MALOMO

Microstructural variations between the bond line and the base alloy of welds have been reported in various nickel-base superalloys that have found their applications as structural materials in aero- and land-based engines. This microstructural variation occurs within 50 to 100 μm of majority of welds. Thus, in order to characterize the strength variations between the weld and the base alloy, mechanical testing at micron level is required. This paper presents the use of a newly developed microtensile testing system for an *in situ* micro-mechanical testing of a powder metallurgy nickel-base superalloy, RR1000 performed in a focused ion beam scanning electron microscope.

DOI: 10.1007/s11661-014-2462-3

I. INTRODUCTION

NICKEL-BASED superalloys are an unusual class of metallic materials with exceptional combination of high-temperature strength, toughness, and resistance to degradation in corrosive or oxidizing environments. These materials are widely used in situation requiring superior strength at high temperatures and consequently find extensive application in the hot sections of gas turbine and rocket engines and nuclear reactors. This high temperature strength is usually provided by a distribution of γ' ($Ni_3(Al,Ti)$) precipitates which hinder dislocation movement.

The need for jet engines to burn fuel more effectively at higher temperatures requires the development of nickel-based superalloys containing increasing amounts of the main strengthening, stable, ordered L12 intermetallic ($Ni_3(Al,Ti)$) γ' phase. Hence, in the last 1 to 2 decades, new polycrystalline nickel-base superalloys have been developed for disk applications operating at high temperatures, containing a significantly higher volume fraction of γ' than previous superalloys (Waspaloy, IN718, Udimet 720, *etc.*). These new alloys (RR1000, René 104, LSHR, Astroloy, Alloy 720Li, N18 *etc.*) have a γ' volume fraction of close to 50 pct.

However, these alloys are very difficult to fusion weld and are prone to heat-affected zone (HAZ) liquation cracking as solidification takes during welding. In order to produce welds with good joint integrity, inertia friction welding (IFW), a nominally solid state welding process, is always used to join gas turbine parts made from these alloys, based on the premise that the joining occurs below the melting point of the bulk material. Furthermore, it is recognized that inertial friction welding is better suited to mass production than electron beam welding since it does not require a vacuum during joining process.[1] But due to the extreme thermo-mechanical history, the microstructure is heavily modified in the HAZ of a joint. Various studies of inertia friction welded nickel-based superalloys in the as-welded condition have shown two different types of hardness profiles in the HAZ. Alloys such as Waspaloy (25 pct γ') and Inconel 718 (25 pct γ'/γ'') generally exhibit a pronounced hardness drop, which is attributed to the absence of γ' in this region after welding while, alloys like N18, Astroloy, Alloy 720Li and RR1000, which contain about 50 pct γ', show a hardness peak in the HAZ.[2,3] Also, it has been reported that macro-tensile properties varies along bond line zone (BLZ) of these nickel-base alloys.[4] Recently microstructural variations between the bond line and the base alloy of welds have been reported in various nickel-base superalloys.[5] Also, the drive to characterize small scale and scale specific properties of materials have been based on the need to reliable predict the performance of microelectro-mechanical systems (MEMS) and other microscale devices. Thus, in order to achieve these mechanical testing at micron level is required. Hence, in this study an *in situ* microtensile test was developed to estimate the strength variations in an inertial friction welded powder metallurgy (PM) nickel-base superalloy.

The development of microscale experiments have been initiated by the need to evaluate mechanical behavior of small volumes of materials and also by a desire to determine how mechanical properties of a material change (if at all they occur) when external dimensions and internal microstructural features are greatly reduced.[6–9] This has been consistently and productively used to predict the performance of MEMS.

Microtensile testing has been extensively studied[5–18] in order to determine the mechanical properties of wide range of materials and to study the importance of size

K.M. OLUWASEGUN, J.O. OLAWALE, M.D. SHITTU, O.O. IGE, Lecturers I, and G.M. OYATOGUN, Senior Lecturer, are with the Department of Materials Science and Engineering, Obafemi Awolowo University, Ile-Ife, Osun State, Nigeria. Contact e-mail: jooolawale@yahoo.com B.O. MALOMO, Lecturer I, is with the Department of Mechanical Engineering, Obafemi Awolowo University.

Manuscript submitted February 6, 2013.
Article published online July 22, 2014

on the mechanical behavior of materials. However, no work has been reported on the mechanical characterization of RR1000 superalloy's welds at micron level. This present work report the use of the developed microtesting system, focused ion beam scanning electron microscope (FIBSEM), and loading directions computed from the Kikuchi maps and pole figure generated by the electron back scattered diffraction (EBSD) in an *in situ* microtensile deformation of RR1000 PM nickel-base superalloy's welds.

II. MATERIALS AND METHODS

A. *Materials*

The material studied is RR1000, a nickel-base superalloy produced by a powder metallurgical route followed by forging. The chemical composition of RR1000 can be found in Table I. As shown in the micrograph of transmission electron microscopy (TEM) in Figure 1, RR 1000 is a precipitation hardened nickel-based superalloy with ~48 vol pct ordered intermetallic phase and average grain size of 6 μm, ranging between 2 and 12 μm. The precipitates are; fairly regular distribution of primary γ' (~0.8 to 4 μm in size), fine (~80 to 220 nm) spheroidal secondary γ' and very fine (~10 to 40 nm) tertiary γ'. According to Pollock and Tin[19] RR1000 have relatively high yield strength in the bulk parent and welded material in the range of 900 to 1300 MPa at room temperature with bulk welded having the highest value.

Table I. Nominal Composition of PM Nickel-Base Superalloy

Element	Composition (wt pct)
Al	3.0
Ti	3.6
Co	18.5
Cr	15.0
Mo	5.0
Zr	0.06
Hf	0.5
Ta	2.0
B	0.015
C	0.027
Ni	balance

B. *Methods*

1. *Sample preparation*

The base material was welded together by IFW, a solid state welding process. Wedge shaped samples were cut from within the parent alloy (parent 1 and 2) and the weld alloy (weld 1 and 2) with electron discharged

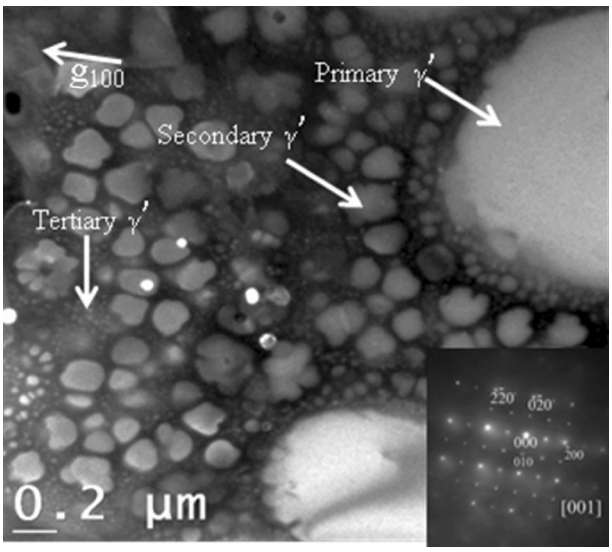

Fig. 1—TEM DF image from the parent alloy showing the trimodal distribution of γ' precipitates.

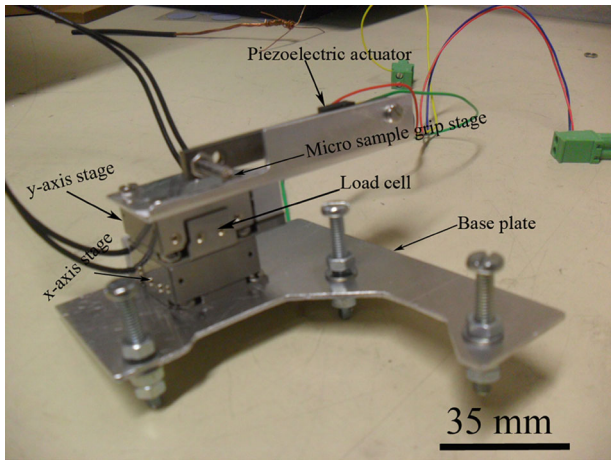

Fig. 2—Photograph of the built microtensile testing system.

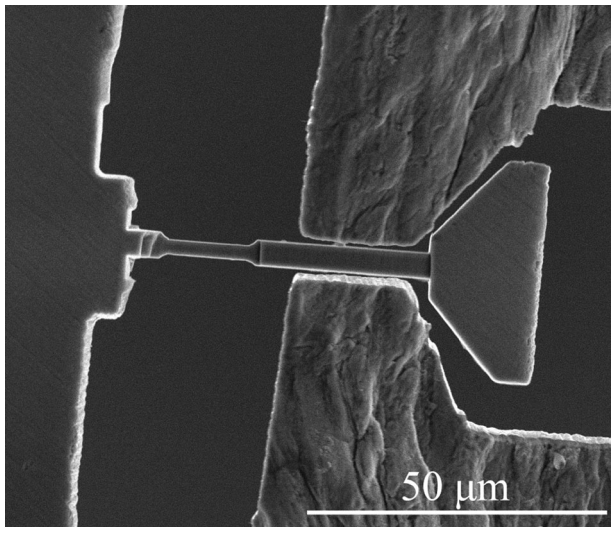

Fig. 3—SEM image showing microtensile sample (13 μm × 2 μm × 3 μm) from base alloy (parent 1) and sample holder aligned before loading in the FIBSEM.

machining (EDM) and polished to a thickness of about 100 μm. The polishing enhances the removal of any re-deposition after EDM. A Quanta 3D FEG SEM FIB with a Ga^+ ion source operated at 30 kV under perpendicular ion impact was carefully used to cut the polished samples into microtensile pieces with 13 μm gauge length. These were finally thinned down to a cross section of 2 μm by 3 μm. Since the samples were machined from polycrystalline bulk material they are single crystals microtensile samples.

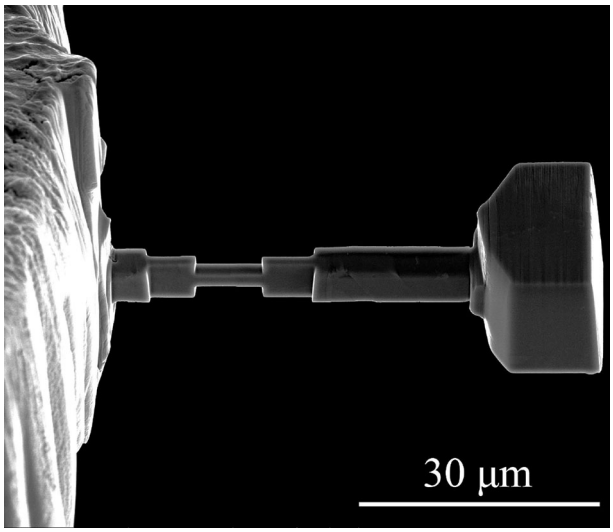

Fig. 4—SEM picture of another FIB microtensile sample (8 μm × 2 μm × 1.7 μm) from the base alloy (parent 2).

Table II. FCC Slip System Identification

Index	Slip Plane	Slip Direction
1	$(11\bar{1})$	[011]
2	$(11\bar{1})$	[101]
3	$(11\bar{1})$	$[1\bar{1}0]$
4	$(1\bar{1}1)$	$[01\bar{1}]$
5	$(1\bar{1}1)$	[101]
6	$(1\bar{1}1)$	[110]
7	$(1\bar{1}1)$	[011]
8	$(1\bar{1}1)$	$[10\bar{1}]$
9	$(1\bar{1}1)$	$[110]$
10	(111)	$[01\bar{1}]$
11	(111)	$[10\bar{1}]$
12	(111)	$[1\bar{1}0]$

2. *Micro-mechanical testing*

The microtensile samples were subsequently tested with *in situ* observation of the microstructures from the scanning electron microscope (SEM). The construction of the microtesting system (Figure 2) used in this study involves a piezo-electric drive used to apply load to the sample through a linear air bearing. Loads were measured using a miniature load cell with an overall load capacity of 0.5 N and a resolution of 0.001 N. Application of load at a load displacement step size of 40 nm gives a corresponding voltage output used to determine the load with a conversion relationship, 100 mV = 1 g.

The microtensile samples were tested *in situ* by pulling to fracture through a load cell attached to a piezoelectric actuator and simultaneously observing the microstructures. Applied load and elongation were measured at different stages of the microtensile test, and this was used to plot the stress–strain curve and analyze together with the recorded SEM images. Elongation was determined by measuring the gauge length within the specimen by using reference marks on the sample from SEM images recorded at each load application stage. The images were recorded *in situ* by in-built video accessory in FIBSEM without interrupting the test after application of load at each stage. From both the *in situ* observation of the formation of slip and the stress–strain results of this test, the yield strength of the samples were determined at the stress level at which the material starts to slip (*i.e.*, when the first slip band was observed *in situ*.), which corresponds to the 0.2 pct offset in the strain. Aside from high accuracy in local positioning through direct visual control; this *in situ* microtensile test also offers insight into the real time material deformation process.

A slight uncertainty in the alignment of the length axis of the sample and the sample holder in the z direction may occur, but we were able to ensure that the flanks of the sample holder and that of the sample head are parallel and equally spaced in order to minimize out-of-plane loading of the specimens as illustrated in Figures 3 and 4. That is load application was applied parallel to the base plate even though Figure 3 looks as if the load application is at an angle. The image looks like that due to the remaining base part of the bulk sample from where the microtensile sample was milled out relative to the base part of the grip.

3. *Evaluation of critical resolved shear stress (CRSS)*

Kikuchi maps and pole figure generated by the EBSD mapping were employed to determine the loading direction and slip plane of the tensile samples, in order to evaluate the critical resolved shear stress (CRSS)

Table III. A Summary of Data from the Microtensile Test (at Room Temperature) of the Parent and As-Welded RR1000 Superalloy

Region	Yield Stress, σ_y (MPa)	Loading Direction	Slip System	Schmid Factor	Critical Resolved Shear Stress, τ_c (MPa)
Parent (1)	619.03	$[\bar{2}00]$	$(\bar{1}11)[\bar{1}\bar{1}0]$	0.4082	252.67
Parent (2)	530.21	$[\bar{5}30]$	$(\bar{1}11)[\bar{1}0\bar{1}]$	0.4803	254.65
Weld (1)	603.68	$[36\bar{1}]$	$(1\bar{1}1)[011]$	0.4970	300.03
Weld (2)	712.50	$[13\bar{3}]$	$(1\bar{1}1)[110]$	0.4297	306.18

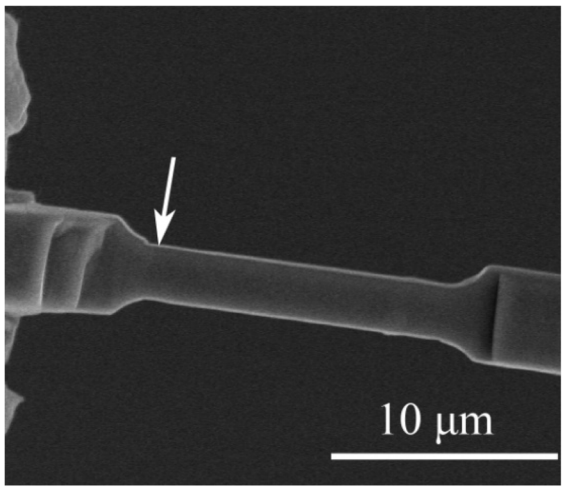

(a) (ε=2.2%)

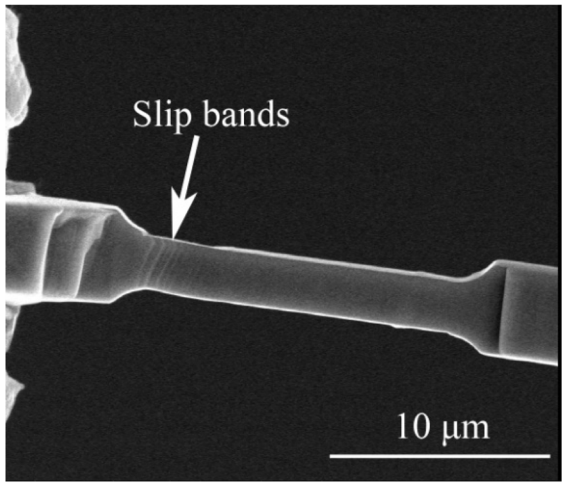

(b) (ε=10.3%)

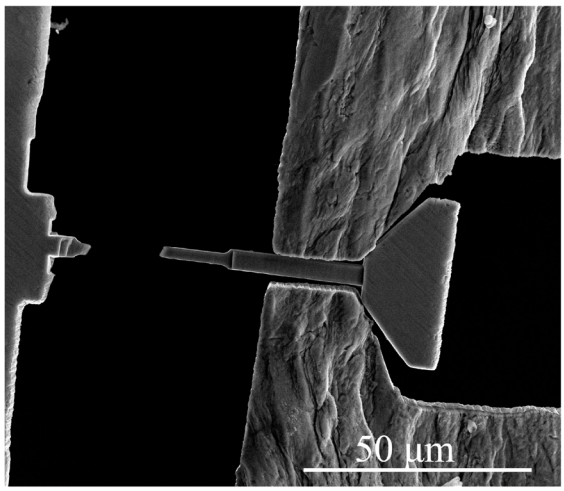

(c)

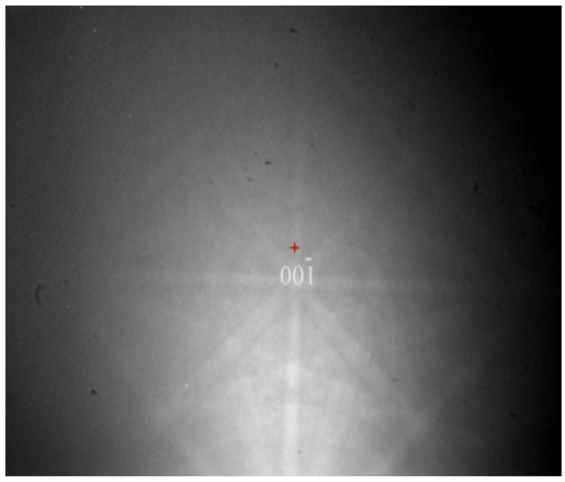

(d)

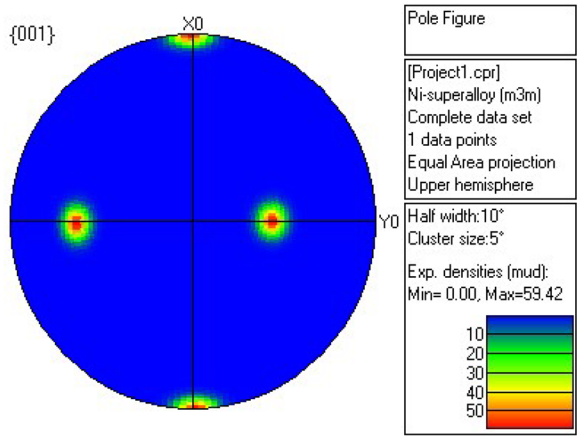

(e)

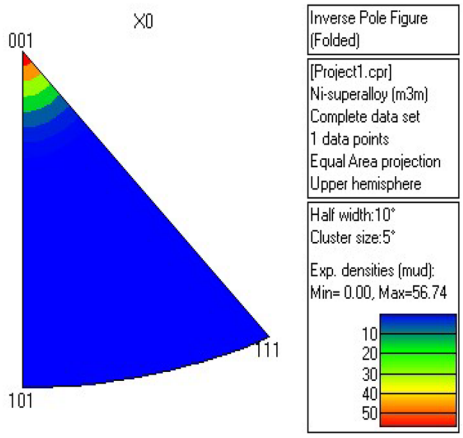

(f)

Fig. 5—Microtensile sample from base alloy (parent 1): (*a*) at 2.2 pct strain, (*b*) during yielding, (*c*) after fracture, (*d*) Kikuchi pattern from the grain where the sample failed, (*e*) pole figure of "d," (*f*) inverse pole figure used to evaluate the loading direction.

operating during the plastic deformation of the microtensile specimens. CHANNEL 5 software (HKL Technology, Denmark) was used to process and analyze the EBSD patterns.

Sample loading direction was determined from the orientation relationship between the microtensile sample coordinates [sample was aligned along the reference rolling direction (Xo) in the SEM] and the crystal coordinates, using EBSD inverse pole figure. Slip plane were determined from the orientation relationship between the slip band on the sample and Kikuchi pattern (plane trace analysis). Since slip direction is on slip plane, $(hkl)\cdot[uvw] = 0$ was used to determine the corresponding slip direction. Table II shows the 12 slip systems in fcc crystal structure. From the slip system Schmid's equation was used to evaluate the CRSS according to Eq. [1]:

$$\tau_c = \sigma_y \cos\alpha \cos\Phi, \qquad [1]$$

where τ_c is the CRSS, σ_y is the yield stress, α is the angle between the stress axis and slip direction, Φ is the angle between the stress axis and normal to slip plane, and $\cos\alpha\cos\Phi$ is the Schmid factor.

The CRSS of the weld and parent material were also evaluated theoretically by characterization of HAZ and

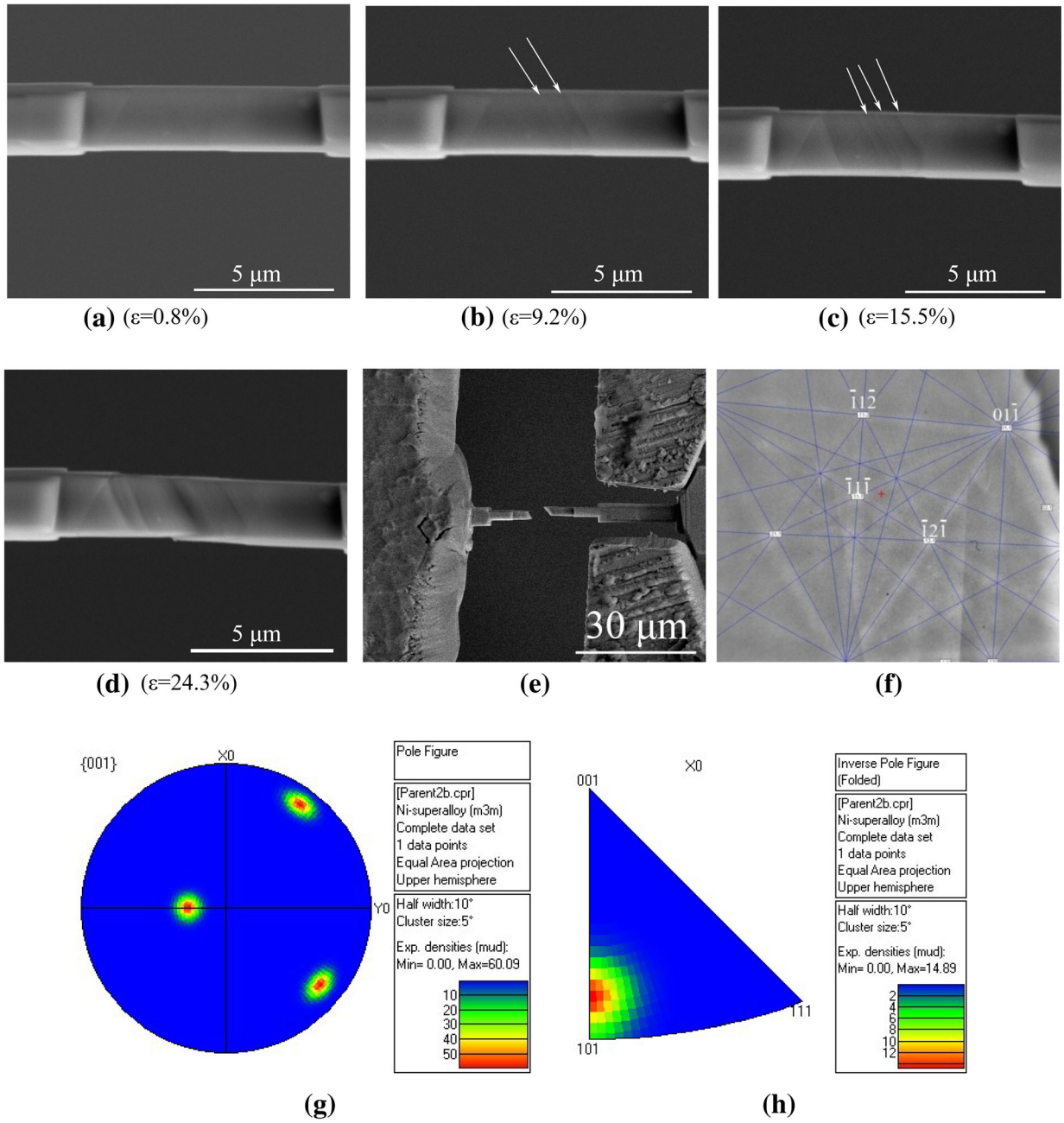

Fig. 6—Microtensile samples from base alloy (parent 2): (*a*) at 0.8 pct strain, (*b*) during yielding, (*c*) and (*d*) showing further deformation, (*e*) after fracture, (*f*) Kikuchi pattern from the grain, (*g*) pole figure of "f," (*h*) inverse pole figure used to evaluate the loading direction.

base alloy using TEM. The values of CRSS obtained from this theoretical evaluation was then compared with experimental value obtained using the pervious procedure.

III. RESULTS AND DISCUSSION

A. *Results*

The summary of the tensile data is presented in Table III. The results indicate yield strength, loading directions, slip system, and CRSS (τ_c) of the parent alloy 1 and 2 and the weld alloy 1 and 2. The CRSS of parent alloy 1 and 2 are the same but their yield strength are different. This same trend is also observed in the weld alloy 1 and 2.

Figures 3 and 4 show a focused ion beam (FIB) prepared microtensile specimen from the parent alloy 1 and 2, respectively. The stages of the deformation of the parent alloy 1 at various strain levels are shown in Figures 5(a) through (c) while that of the parent alloy 2 are shown in Figures 6(a) through (e). The material was observed to yield at a stress level of 619.03 MPa (Figure 7) and 530.21 MPa (Figure 8) for parent alloy 1 and 2, respectively. Figures 7 and 8 are the stress *vs* strain plot of the parent material. From these curves the values of yield strength were determined at value correspond to 0.2 pct offset but the values of ultimate tensile strength (UTS) cannot be determined because a conspicuous necking was not observed before fracturing and this is the limitation of this work. Also, the stress–strain curve of parent material 1 (Figure 7) is higher than parent material 2 (Figure 8) which is an indication that modulus of elasticity of parent material 1 is higher than parent material 2. This variation can be attributed to the different orientations of grains from where the samples were machined.

The loading direction of parent alloy 1 computed from the Kikuchi maps (Figure 5(d)) and the pole figure generated by the EBSD mapping (Figures 5(e) and (f)); using HKL Channel 5 software is $[\bar{2}00]$. The sample yielded at a stress level 619.03 MPa on slip plane $(\bar{1}11)$ and slip direction $[\bar{1}0\bar{1}]$. The calculated CRSS for the loading direction and slip system was 252.67 MPa. Similarly, parent alloy 2 was determined on the loading direction of $[\bar{5}30]$ as computed from the Kikuchi maps (Figure 6(f)) and the pole figure generated by the EBSD mapping (Figures 6(g) and (h)), using HKL Channel 5 software. The sample yielded at a stress level of 530.21 MPa on slip plane $(\bar{1}11)$ and slip direction $[\bar{1}0\bar{1}]$. The CRSS calculated from the determined slip system and the loading axis was 254.65 MPa, which is consistent with the value obtained for the parent alloy 1.

Figures 9(a) and 10(a) show a FIB prepared microtensile specimen from the weld alloy 1 and 2, respectively. The stages of the deformation of the weld alloy 1 and 2 at various strain levels are shown in Figures 9(b) through (e) and 10(b) through (e). The weld alloy 1 was observed to yield at a stress level of 603.68 MPa (Figure 11) while weld alloy 2 at 712.50 MPa (Figure 12). Figures 11 and 12 are the stress–strain plot of the weld alloy. Like parent material

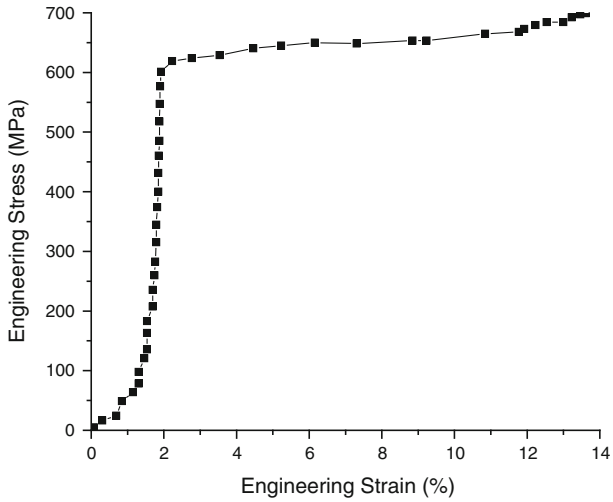

Fig. 7—Stress–strain curve of the microtensile specimen prepared from the base alloy (parent 1).

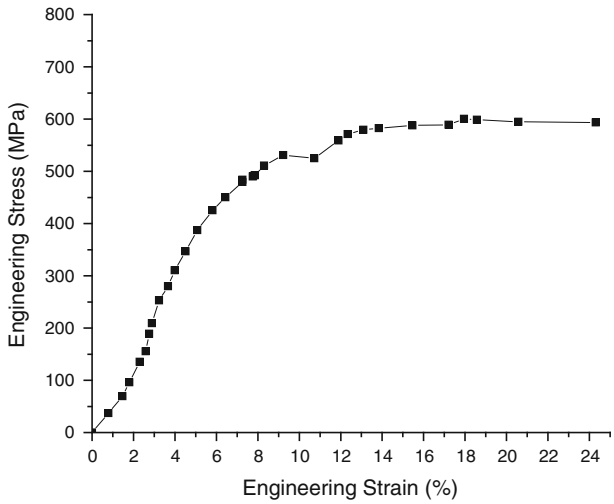

Fig. 8—Stress–strain curve of the microtensile specimen prepared from the base alloy (parent 2).

the values of yield strength were determined at value correspond to 0.2 pct offset while UTS cannot be determined because a conspicuous necking was not observed before fracturing. Also, the strain hardening observed in Figure 12 is more than Figure 11. This can be as a result of the twist that occurred during the deformation of the weld alloy 2 as observed in its SEM image (Figure 10).

Within the BLZ of the weld alloy (weld 1), the microtensile sample was loaded in $[3\bar{6}\bar{1}]$ direction as computed from the Kikuchi maps (Figure 9(f)) and the pole figure generated by the EBSD mapping (Figures 9(g) and (h)), using HKL Channel 5 software. The sample yielded at a stress level of 603.68 MPa (Figure 11) on two slip planes (111) and $(1\bar{1}1)$ and slip directions $[1\bar{1}0]$ and [011], respectively, with a CRSS of 300.03 MPa. The second weld alloy (weld 2) from the BLZ was loaded in $[13\bar{3}]$ direction as computed from the Kikuchi maps (Figure 10(f)) and the pole figure generated by the EBSD mapping (Figures 10(g) and (h)),

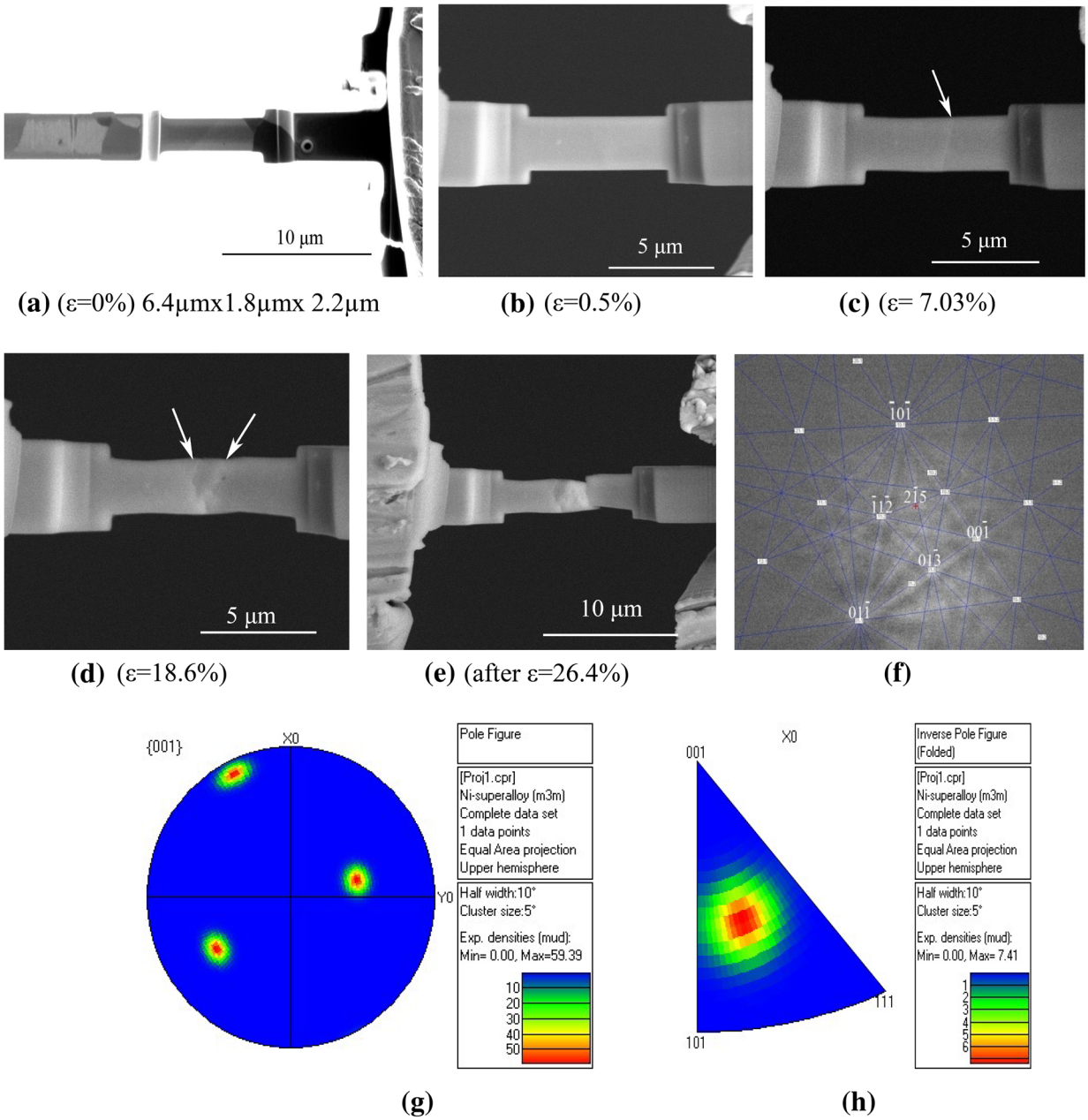

Fig. 9—Microtensile sample from BLZ of weld (1) showing ((*a*) through (*e*)) microstructures at various strain levels, illustrating the initiation of slip steps and the fracture of the sample, (*f*) Kikuchi pattern from the grain within the sample gauge length, (*g*) pole figure of "f,"(*h*) inverse pole figure used to evaluate the loading direction.

using HKL Channel 5 software. The sample yielded at 712.50 MPa (Figure 12) on slip plane ($(1\bar{1}1)$ and slip directions [110] with a CRSS of 306.18 MPa. The CRSS obtained for this sample (weld 2) is also consistent with the CRSS in the first microtensile sample from the BLZ (weld 1). This consistency in the values is evidence that this microtensile testing is feasible for testing localized strength in this class of material.

The microstructure of the weld in HAZ as revealed by TEM is presented in Figure 13. The microstructure revealed that re-precipitated tertiary γ' is within 0.3 mm of HAZ of the weld (Figure 13(a)) and tri-modal γ' precipitate is within 4.5 mm of the base material (Figure 13(c)). The precipitates distance, grain size and volume fraction within the matrix were quantified by image J software (Figures 13(b) and (d)). With this software the volume fraction and grain diameter of tertiary γ' precipitate within the weld was estimated as 19 pct and 40 nm, respectively (Figure 13(b)), while the volume fraction of tertiary γ' precipitate within the base material as 8 pct (Figure 13(d)).

B. *Discussion*

Weld regions in γ' strengthened nickel-base alloys have been reported to possess higher yield strength than the base alloy. This was related to the re-precipitation of high volume fraction of tertiary γ' (10 to 40 nm in size)

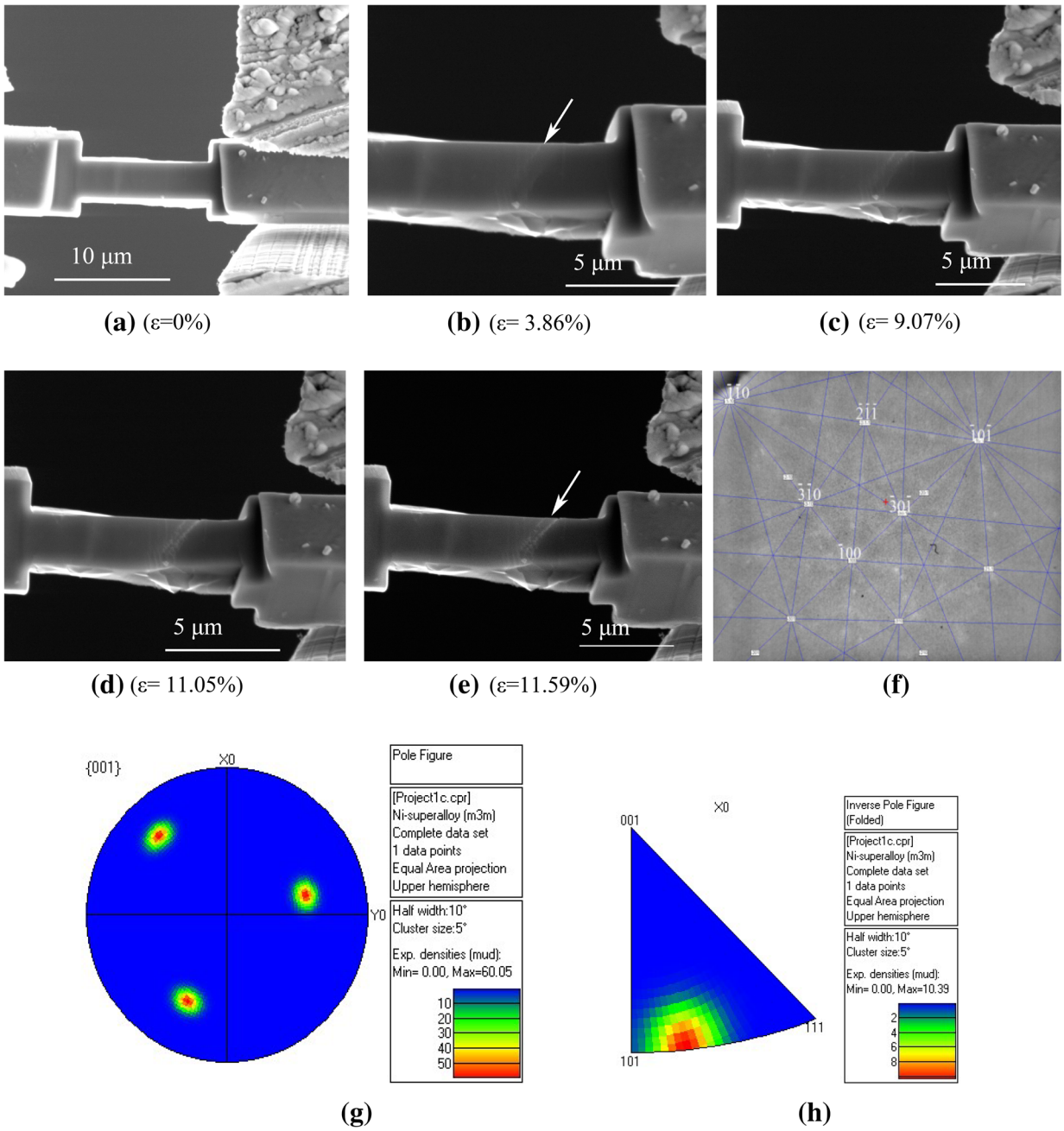

Fig. 10—Microtensile sample from BLZ of another weld (2) showing ((*a*) through (*e*)) microstructures at various strain levels, illustrating the initiation of slip, (*f*) Kikuchi pattern from the grain within the sample gauge length, (*g*) pole figure of "f," (*h*) inverse pole figure used to evaluate the loading direction.

within the grains of the weld, which impede the motion of dislocation.[19,20] However, this expected trend in the yield strength of the base alloy and the weld may not be directly applicable to microtensile samples with single crystal, due to the effect of crystal orientation with respect to the stress axis on the resultant strength of the tested single crystal material. For example the yield strength of the parent sample (1) is greater than the yield strength of weld sample (1), but reverse is the case for their CRSS.

Plastic deformation in materials at micro or atomic scale is evident by the formation of slip. The slip begins on a given system (plane and direction) when the shear stress resolved on that system reaches a critical value (Schmid's law). Thus, it is suggested that CRSS is the appropriate parameter to use in comparing the strength of the base alloy and the weld in single crystal microtensile samples prepared from a polycrystalline bulk material, since this takes into account the orientation relationship between the crystal and the sample loading axis.

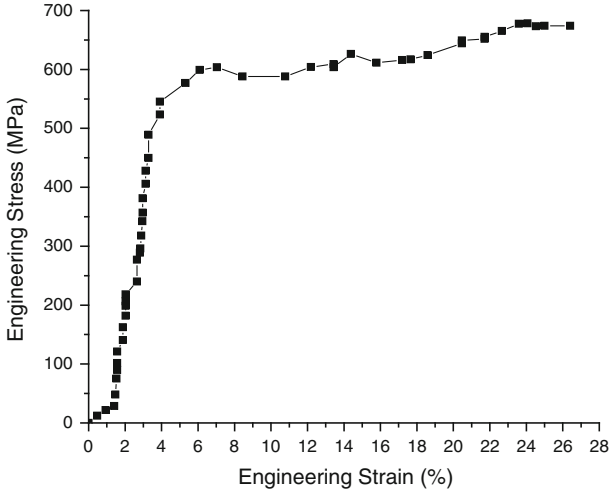

Fig. 11—Stress–strain curve of the microtensile specimen prepared from the weld.

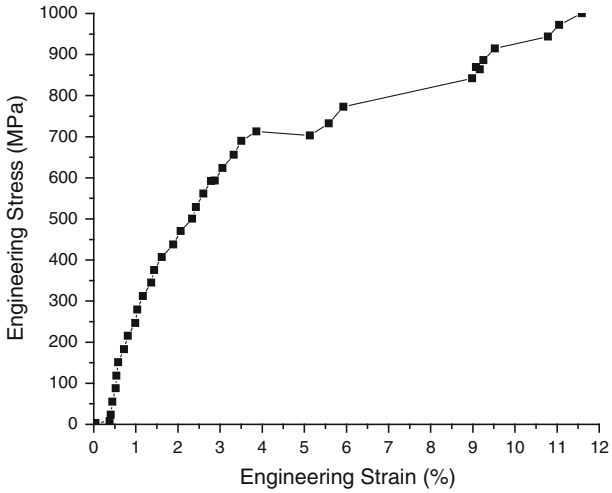

Fig. 12—Stress–strain curve of the microtensile specimen prepared from the second weld region.

Table III clearly shows that the resolved shear stress of the weld is higher than the base alloy, which means that the weld is stronger than the base material. This is consistent with the trend of the yield strength from the bulk tensile samples, and can be attributed to the inhibiting effect for dislocation motion (restricting the plastic flow) offered to the weld by the fine and highly dense coherent re-precipitated tertiary γ' precipitates reported in other works.[19,21] However, it is noteworthy to state here that the measured yield strength in the microtensile samples is lower than the expected yield strength in bulk materials, this discrepancy in the values could be as a result of size and crystallographic orientation effect of microtensile sample on the yield strength.[9,22,23]

The experimental CRSS results from this work have shown consistency with estimated CRSS from precipitates hardening models proposed by Huther and Rappich,[24] and Brown and Ham.[25] The model is based on the premise that the deformation of γ' precipitation hardened nickel alloys at room temperature is governed by two coupled edge dislocation moving in the $\langle 110 \rangle$ direction on the $\{111\}$ plane. According to the model, for small tertiary γ', the CRSS is determined by the stress necessary to move weakly coupled dislocation pairs through the γ' precipitate and it is given in Eq. [2]:

$$\tau_c = \frac{1}{2}\left(\frac{\Gamma}{\mathbf{b}}\right)^{\frac{3}{2}}\left(\frac{\mathbf{b}df}{T}\right)^{\frac{1}{2}}A - \frac{1}{2}\left(\frac{\Gamma}{\mathbf{b}}\right)f, \qquad [2]$$

where Γ is the anti-phase domain boundary energy (APBE) of the γ' particles in the $\{111\}$ plane, which is taken as 0.28 J m^{-2},[26] $\mathbf{b}$ is the Burgers vector of the edge dislocation in the γ matrix ($\mathbf{b} = 1/2[110]\ a_o$, $a_o =$ 3.55 Å), d is the particle diameter, f is the volume fraction of the γ' precipitates, T is the line tension of the dislocation, $T = \left(\frac{G\mathbf{b}^2}{2}\right)$, G is the isotropic elastic shear modulus, which is taken as 80 GPa,[26] A is a numerical factor depending on the morphology of the precipitates. For spherical precipitates the value of A is taken as 0.72.[27]

Taking other parameters as following, $f =$ 19 pct (as determined within 0.3 mm of the weld (refer to Figures 13(a) and (b)), $d =$ 40 nm (maximum diameter of the γ' observed within the weld (Figures 13(a) and (b)), we have $\tau_c =$ 308.3 MPa. This theoretical value is consistent with the experimental value of CRSS in this work, suggesting that tertiary γ' could be responsible for the strength of the weld, as also dictated by the microstructure within 0.3 mm of the weld in Figures 13(a) and (b).

It may be difficult to use this model for the CRSS within the parent material due to the complexity that may be involved with the variations in the diameter of the tri-modal precipitates co-existing in the parent material. However, to ensure consistency in the size of the precipitate for the model, the evaluation of CRSS in the parent material will be assumed to be based on the fraction of the tertiary γ' in the parent material. The volume fraction for tertiary γ' has been measured to be 8 pct (refer to Figures 13(c) and (d)). Using this value in the model gives; $\tau_c =$ 224.2 MPa, which is also close to the experimental value. This results, therefore, suggest that it is reasonable to attribute the change of CRSS of the welded specimen to the evolution of the tertiary γ'.

IV. SUMMARY

The results of the microtensile tests have shown that the developed *in situ* microtensile test can be used to estimate the strength variations in a solid state welded PM nickel-base superalloy. The results have also shown that the CRSS within the weld region is higher than that of the base alloy. Hence, CRSS is the appropriate parameter to use in comparing the strength of the base alloy and the weld in single crystal microtensile samples prepared from a polycrystalline bulk material.

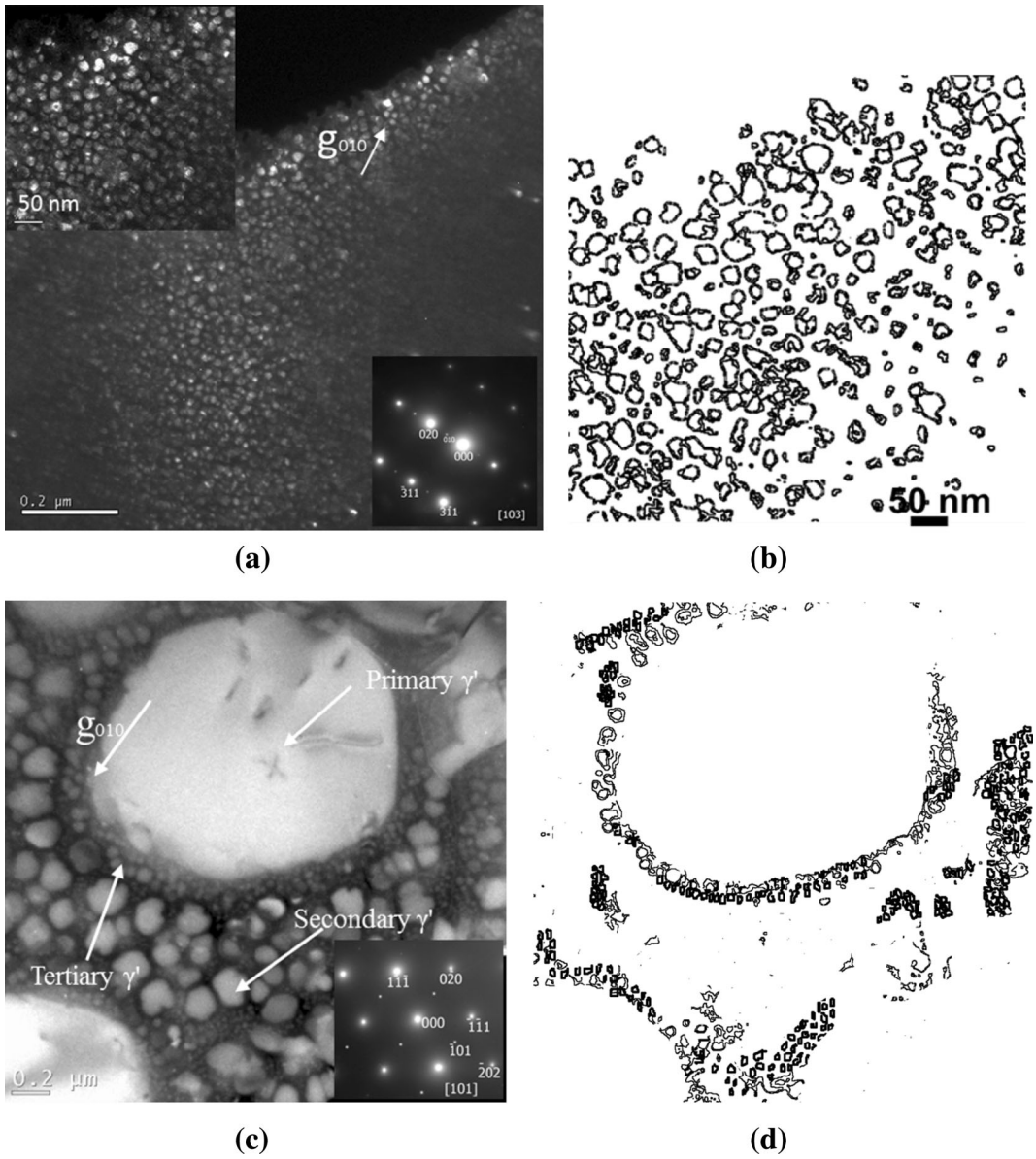

Fig. 13—TEM DF image of (*a*) re-precipitated tertiary γ' within 0.3 mm of HAZ of the weld, (*b*) representative image J software output of tertiary γ' (19 pct volume fraction) for the inset in "a," (*c*) TEM DF image of the trimodal γ' precipitate, 4.5 mm away from the bond line (*i.e.*, within the base material), (*d*) representative image J software output of tertiary γ' (8 pct volume fraction) in "c".

REFERENCES

1. R. Spinat and Y. Honnorat: in *High Temperature Alloys for Gas Turbines and Other Applications*, W. Betz, R. Brunetaud, D. Coutsouradis, H. Fischmeister, T.B. Gibbons, I. Kverness, Y. Lindblom, J.B. Marriott, and D.B. Meadowcroft, eds., D. Reidel, Dordrecht, 1986, pp. 151–57.
2. M. Preuss, J.W.L. Pang, P.J. Withers, and G.J. Baxter: *Metall. Mater. Trans. A*, 2002, vol. 33A, pp. 3115–25.
3. M. Preuss, J. Quinta da Fonseca, I. Kyriakoglou, P.J. Withers, and G.J. Baxter: in *10th Int. Sympos. Superalloy 2004*, K.A. Green, ed., TMS, Seven Springs, Champion, PA, 2004, pp. 477–84.
4. M. Preuss, P.J. Withers, and G.J. Baxter: *Mater. Sci. Eng. A*, 2006, vol. 437, pp. 38–45.
5. K.M. Oluwasegun, M.O. Adeoye, A.A. Adeleke, B. Aremo, and A.V. Adedayo: *Niger. J. Mater. Sci. Eng.*, 2012, pp. 15–23.
6. T. Yi and C.J. Kim: *Meas. Sci. Technol.*, 1999, vol. 10, pp. 706–16.
7. W.N. Sharpe: in *International Semiconductor Device Research Symposium, Proceedings, 2001*, pp. 416–17.
8. S.M. Spearing: *Acdedata Mater.*, 2000, vol. 48, pp. 179–96.
9. M.A. Haque and M.T.A. Saif: *Exp. Mech.*, 2003, vol. 43, pp. 248–55.
10. K.J. Hemker and W.N. Sharpe: *Annu. Rev. Mater. Res.*, 2007, vol. 37, pp. 93–126.
11. M. Zupan and K.J. Hemker: *Metall. Mater. Trans. A*, 1998, vol. 29A, pp. 65–71.
12. K.J. Hemker, M. Lu, and M. Zupan: *Struct. Intermet.*, 1997, vol. 1996, pp. 147–56.
13. M. Zupan, M.J. Hayden, C.J. Boehlert, and K.J. Hemker: *Exp. Mech.*, 2001, vol. 41, pp. 242–47.
14. E.H. Klaassen, K. Petersen, J.M. Noworolski, J. Logan, and N.I. Maluf: *Sens. Actuators A*, 1996, vol. 52, pp. 132–39.
15. W.N. Sharpe, B. Yuan, R. Vaidyanathan, and R.L. Edwards: *Microlithogr. Metrol. Micromach. II*, 1996, vol. 2880, pp. 78–91.
16. W.N. Sharpe, K.T. Turner, and R.L. Edwards: *Exp. Mech.*, 1999, vol. 39, pp. 162–70.

17. D.A. LaVan and W.N. Sharpe: *Metall. Mater. Trans. A*, 2001, vol. 32A, pp. 913–22.
18. D.S. Gianola, S. Van Petegem, M. Legros, S. Brandstetter, H. Van Swygenhoven, and K.J. Hemker: *Acta Mater.*, 2006, vol. 54, pp. 2253–63.
19. T.M. Pollock and S. Tin: *J. Propuls. Power*, 2006, vol. 22 (2), pp. 361–73.
20. R.J. Mitchell, M. Preuss, S. Tin, and M.C. Hardy: *Mater. Sci. Eng. A*, 2008, vol. 473, pp. 158–65.
21. M. Preuss, J.W.L. Pang, P.J. Withers, and G.J. Baxter: *Metall. Mater. Trans. A*, 2002, vol. 33A, pp. 3215–25.
22. M.A. Haque and M.T.A. Saif: *Scripta Mater.*, 2002, vol. 47, pp. 863–67.
23. M.A. Haque and M.T.A. Saif: *Exp. Mech.*, 2002, vol. 42, pp. 123–28.
24. W. Huther and B. Reppich: *Zeitschrift Fur Metallkunde*, 1978, vol. 69, pp. 628–34.
25. L.M. Brown and R.K. Ham: *Strengthening Mechanisms in Crystals*, Applied Science, London, 1971.
26. M.P. Jackson and R.C. Reed: *Mater. Sci. Eng. A*, 1999, vol. A259, pp. 85–97.
27. B. Reppich: *Acta Metall.*, 1982, vol. 30, pp. 87–94.